Arreyndip, Nkongho Ayuketang; Ebobenow, Joseph

Article

Small 500 kW onshore wind farm project in Kribi, Cameroon: Sizing and checkers layout optimization model

Energy Reports

Provided in Cooperation with:
Elsevier

Suggested Citation: Arreyndip, Nkongho Ayuketang; Ebobenow, Joseph (2018) : Small 500 kW onshore wind farm project in Kribi, Cameroon: Sizing and checkers layout optimization model, Energy Reports, ISSN 2352-4847, Elsevier, Amsterdam, Vol. 4, pp. 528-535, https://doi.org/10.1016/j.egyr.2018.08.003

Energy Reports 4 (2018) 528–535

Contents lists available at ScienceDirect

Energy Reports

journal homepage: www.elsevier.com/locate/egyr

Research paper

Small 500 kW onshore wind farm project in Kribi, Cameroon: Sizing and checkers layout optimization model

Nkongho Ayuketang Arreyndip [a,b,c,*], Ebobenow Joseph [a]

[a] Department of Physics and Applied Physics, University of Buea, 63, Buea, Cameroon
[b] African Institute for Mathematical Science (AIMS), Limbe, Cameroon
[c] Polytechnic, Saint Jerome Catholic University of Douala, 5949, Akwa, Douala, Cameroon

ARTICLE INFO

Article history:
Received 30 January 2018
Received in revised form 18 May 2018
Accepted 20 August 2018
Available online 6 September 2018

Keywords:
Wind farm
Layout
Optimization

ABSTRACT

For the purpose of providing cheap, affordable and reliable electrical energy to communities in need and power-up new industries and enterprises, a small onshore wind farm with an estimated capacity of 500 kW is designed and studied. With the help of a wind rose, wind resource map, and results from Weibull statistics, a potential site is selected and the wind farm is positioned along Cameroon's coastline for maximum energy capture. Using the PARK model for wind turbine layout optimization, two different layout patterns (Checkers pattern and column pattern) are studied for the purpose of minimizing the wake effect and thereby, maximizing the output power from the farm. The Checkers model was found suitable as compared to the column model to be used on Grand Batanga, a small locality South of the city of Kribi, Cameroon.

1. Introduction

The quest to become an emerging state by the year 2035 has pushed Cameroon's government to heavily invest in the energy sector, as energy is the driving force behind the rapid development of any country. Significant progress has already been made with a newly constructed dam in the south region of the country. But giving that dams are not ecologically friendly and also given problems posed by global warming with the earth warming by 1° every 10 years, has caused most sub-saharan African countries like Cameroon to be affected by droughts. Long periods of droughts or dry season as is often the case in the tropics give rise to seasonal rivers. Hence there is usually very low energy output from these dams during the dry seasons which causes some large communities to go days and sometimes weeks without electricity.

Our objective in this work is to contribute in the energy sector by identifying potential renewable energy sources, sites and propose efficient ways of harnessing them that can add significant megawatts to the national grid. Which will go a long way to make electrical energy available in rural areas that are often forgotten or deprived of basic energy and water.

For a larger and more industrious community like Kribi, wind energy has been found suitable as an alternative energy source compared to solar in Cameroon because it is cheaper and yields more power per square area of land than solar.

To select the best site for the installation of a small wind farm, the first step is to carry out a wind energy assessment which is usually done using wind resource maps. A wind resource map for Cameroon is shown in Fig. 1 (Anon, 2014). Here we see that favourable wind speeds to support a small wind farm are mostly available in the Northern parts of the country and the coastal regions. Also given that the population density in the coastal regions is increasing in an alarming rate and more industries and enterprises are being created in these regions, we choose to look for a potential wind energy site for the installation of a small wind farm along the coast.

Next we have applied the Weibull statistics to estimate and compare the wind power densities, average wind speeds, most probable wind speeds and wind speed carrying maximum energy of three different locations in three different coastal regions to select the best site with sufficient wind speed (Arreyndip et al., 2016). When the best site is selected, next step is to select an appropriate wind turbine with wind speed characteristics capable of fully functioning on the chosen site and finally given the energy needs of the consumer, a wind farm is constructed to satisfy these energy needs.

To construct a wind farm, wind turbines layout within the farm is a very crucial step towards harvesting higher energy from the farm as wrong positioning leads to maximizing the wake effect and minimizing power capture. The problem of wake (which is a low wind field created by a wind turbine that is sometimes

* Corresponding author at: Department of Physics and Applied Physics, University of Buea, 63, Buea, Cameroon.
E-mail address: ayuketang@aims-cameroon.org (N.A. Arreyndip).

https://doi.org/10.1016/j.egyr.2018.08.003

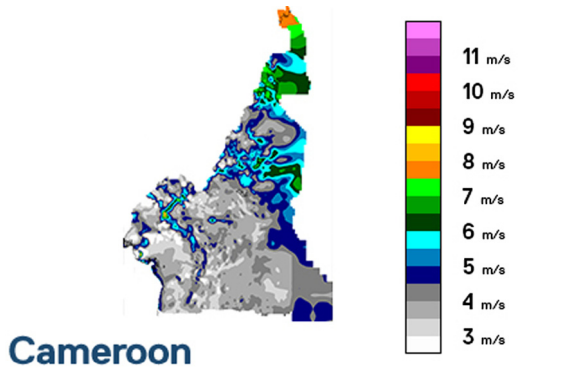

Fig. 1. Wind resource map of Cameroon showing distribution of wind speed over the territory (Anon, 2014).

experienced by another wind turbine downstream) elimination in a large wind farm with clusters of large wind turbines still remains a challenge (Wang et al., 2016b; Kusiak and Song, 2010; Song et al., 2013). But this challenge can equally be eliminated by the constructing stand-alone wind turbines farm that will definitely take an incredible land space. Hence given that we are constrained in a particular land surface area, researchers have developed and simulated complex wake models to solve the wake problem (Wang et al., 2016b; Kusiak and Song, 2010; Song et al., 2013). They have shown that an efficient wind farm design can be carried out through optimization of wind farm layout and also carrying out some control strategies (Wang et al., 2016b; Kusiak and Song, 2010; Song et al., 2013). Which can go a long way to minimize the wake effect by cutting down power loses due to turbulence and maximize the wind farm output power.

Here, we will limit ourselves to simple analytic wake models without going deeply into Computational Fluid Dynamics (CFD) simulation since we do not have access to the software. More complex wake models have been developed like the Ainslie-based models, the parabolic Navier–Stokes (N–S) equation and the complete 3D (N–S) models (Wang et al., 2016b). Researchers who have already developed and studied different analytic models for wind farm layout optimization are; Longyan et al. applied and compared the effectiveness of three different analytic wake models (PARK, Larsen and B–P model) for wind farm with variable and constant hub heights. One of their result is that, when using PARK model, the surface roughness value must be carefully tuned to achieve good performance in predicting the wind farm power production (Wang et al., 2016b). Kusiac and Song also applied the PARK model for the purpose of maximizing output power from a circular shape wind farm. Their complex nonlinear model was solved by the evolutionary strategy algorithm with the quality of the generated solutions acceptable for industrial applications (Kusiak and Song, 2010).

In this work, we will limit ourselves to the most popular and widely used wake model for wind farm layout optimization which is the PARK model and focus more on wind turbine sizing and the layout patterns with minimal wake effects. The remaining sections are organized and explained as follows. In Section 2, we will revisit the widely used Weibull model for wind energy assessment, the actuator disc concept and the PARK model. We will also make use of the wind rose which will help us in positioning wind turbines in the farm. Sizing and layout patterns over the selected site for maximum energy capture are also discussed. Wind power output will also ba calculated and compared using the different layout patterns. Section 3 is dedicated to discussing the results of our findings and we will end with a conclusion in Section 4.

2. Methods

We will start this section with a brief review of the widely used Weibull statistics for wind energy assessment in which we have already presented some results which are stated here-in in our previous work. We will also revisit the actuator disc concept and the PARK model which will help readers without a background in wind energy to know how and where some constants and parameters like the axial induction factor, power coefficient are derived and assigned values.

2.1. Weibull statistics

The Weibull distribution with probability density function, cumulative probability distribution and quantile distribution given by (Arreyndip et al., 2016; Fagbenle et al., 2011; Oyedepo et al., 2012; Kollu et al., 2012; Ozerdem and Turkeli, 2003; Carta et al., 2009; Montgomery and Runger, 2003; Akpinar and Akpinar, 2005; Arreyndip and Joseph, 2016):

$$f(v) = \left(\frac{k}{c}\right)\left(\frac{v}{c}\right)^{k-1} \exp\left[-\left(\frac{v}{c}\right)^{k}\right], \tag{1}$$

$$F(v) = 1 - \exp\left(-\left(\frac{v}{c}\right)^{k}\right), \tag{2}$$

$$Q(v) = [-\log(1-v)]^{\frac{1}{k}}. \tag{3}$$

The mean value of the wind speed v_m and standard deviation ν is defined in terms of the Weibull parameter k and c are given as (Arreyndip et al., 2016; Fagbenle et al., 2011):

$$v_m = c\Gamma\left(1 + \frac{1}{k}\right), \tag{4}$$

where $\Gamma()$ is the gamma function. and

$$\nu = \sqrt{c^2\left[\Gamma\left(1+\frac{2}{k}\right) - \left[\Gamma\left(1+\frac{1}{k}\right)\right]^2\right]}. \tag{5}$$

2.1.1. Mean power and energy densities

When assessing the wind energy potential of a site, there are two wind speeds that are of interest and must therefore be taken seriously into consideration. These are the most probable wind speed v_{mp} and the wind speed carrying maximum energy v_{Emax}. They are given by the expression (Oyedepo et al., 2012; Kollu et al., 2012):

$$v_{mp} = c\left(\frac{k-1}{k}\right)^{(1/k)}, \tag{6}$$

and

$$v_{Emax} = c\left(\frac{k+2}{k}\right)^{(1/k)}. \tag{7}$$

Theoretically, the mean power density is proportional to the cube of the mean velocity given by,

$$P_D = \frac{P(v_m)}{A} = \frac{1}{2}\rho v_m^3. \tag{8}$$

It can also be calculate from the Weibull probability density function given by,

$$P_D = \frac{P(v)}{A} = \frac{1}{2}\rho c^3\Gamma\left(1+\frac{3}{k}\right), \tag{9}$$

and the energy density is given by,

$$E_D = \frac{1}{2}\rho c^3\Gamma\left(1+\frac{3}{k}\right)T. \tag{10}$$

Table 1
Data descriptive statistics.

Data	Kribi	Douala	Limbe
min (m/s)	1	0.8	1.45
max (m/s)	6.45	3.45	4.62
median (m/s)	2.3	1.6	2.04
mean (m/s)	2.5	1.7	2.31
s.d	0.87	0.43	0.7
skew	1.45	0.9	1.35
kurt	5.17	4.43	3.88
p-value	2.011e−10	2.89e−05	4.19e−09

Table 2
Wind characteristics of coastal regions.

Data	Kribi	Douala	Limbe
Longitude	9.98	9.7	9.21
Latitude	2.88	4.05	4.02
Elevation (m)	15	41	36
v_{mp} (m/s)	2.426	1.67	2.27
v_{max} (m/s)	3.35	2.0	3.30
P_D (W/m^2)	33.7	8.0	25.42
P_{max} (W/m^2)	160	30	60

Where P_D is the power density, E_D the energy density, $P(v)$ wind power, A cross sectional area of rotor, ρ the air density assumed here to take the value 1.225, c scale parameter, k shape parameter, T period, and $\Gamma()$ the gamma function (Fagbenle et al., 2011; Oyedepo et al., 2012; Kollu et al., 2012). The shape and scale parameters here, have been estimated from the maximum likelihood method given by the expressions:

$$shape(k) = \left[\frac{\sum_{i=1}^{n} v_i^k \ln(v_i)}{\sum_{i=1}^{n} v_i^k} - \frac{\sum_{i=1}^{n} \ln(v_i)}{n}\right]^{-1}, \tag{11}$$

where v_i is the wind speed in time step i and n is the number of data points.

The scale parameter is given by (Fagbenle et al., 2011):

$$scale(c) = \left[\frac{1}{n}\sum_{i=1}^{n} v_i^k\right]^{1/k}. \tag{12}$$

The data set used in the previous work (Arreyndip et al., 2016) is NASA satellite wind data over Limbe, with latitude 4.02°N, longitude 9.21°E and elevation of about 69 m above sea level, Douala with longitude 9.76°E, latitude 4.05°N and with an elevation of 19m above sea level and Kribi with longitude 9.98°E, latitude 2.88°N with an elevation of 10 m above sea level. These data sets contains 31 (1983–2013) years of mean daily data with missing values in the years 1992 and 1994 for the Limbe data which is taken at Debouncha, on the western coast of Limbe. Hence these years were considered as outliers.

The results of the parameter estimation, mean power densities, maximum power densities, most probable wind speeds and wind speed carrying maximum energy over three of Cameroon's coastal cities have already been presented in our previous work (Arreyndip et al., 2016) but displayed in Tables 1–3 and Fig. 2 for clarity. Fig. 3a and b are the probability density function (PDF) and cumulative distribution function (CDF) of NASA mean monthly data of Kribi fitted to Weibull distribution (Arreyndip et al., 2016).

From Tables 1–3 and comparative plots for Weibull power density in Fig. 2, we see that Kribi is the best site given that it has a higher Weibull power density and mean wind speed. But we also see that wind speed in Kribi that is estimated about 3 m/s is very low to support a modern large wind turbine energy farm. Hence small wind turbines with cut-in wind speed a little lower than the mean speed over Kribi are employed to construct the wind farm.

Table 3
Summary statistics for Weibull fit using the method of maximum likelihood.

Data	Kribi	Douala	Limbe
k	2.9	3.9	3.0
s.e	0.1	0.14	0.128
c (m/s)	2.8	1.8	2.58
s.e (m/s)	0.05	0.026	0.05
likelihood	−475.6	−232.27	−333.17
P-value of K–S	0.14	0.118	0.18

2.2. Actuator disc theory

The actuator disc concept is based on the fact that a rotating rotor produces a disclike structure that spins wind in circular direction behind the turbine to produce a stream tube shown in Fig. 4 (Castellani et al., 2013; Archer et al., 2013). This aerodynamic simulation gives us an idea about the variation of wind speeds and pressure before and after the rotating rotor. The resulting spinning velocity behind the rotor is what is called the wake which greatly affects wind turbines positioned downstream as their power capture drops because of turbulence.

Let us consider the actuator disc shown in Fig. 4. The velocity and pressure in front of the disc are denoted as v_u and P_0^+ respectively. While those behind the disc are denoted as v_w and P_0^- respectively (Munteanu et al., 2014). Momentum change across the wind turbine is given by,

$$\triangle T = m(v_u - v_w), \tag{13}$$

which is the momentum transmitted to the disc by air of mass m passing through the disc with cross sectional area A. The force on the blades due to this momentum change is then given by (Munteanu et al., 2014):

$$F = \frac{\triangle T}{\triangle t} = \frac{\triangle m(v_u - v_w)}{\triangle t} = \rho A v_0 (v_u - v_w). \tag{14}$$

The force can also be written in the form

$$F = A(P_0^+ - P_0^-), \tag{15}$$

and also making use of the Bernoulli's equation, the pressure difference is given by (Munteanu et al., 2014):

$$P_0^+ - P_0^- = \frac{1}{2}\rho(v_u^2 - v_w^2). \tag{16}$$

Immediately before and after the disc, $v_0 = v_u$ and $v_0 = v_w$ respectively, the force is then given by,

$$F = \frac{1}{2}\rho A(v_u^2 - v_w^2). \tag{17}$$

Using Eqs. (14) and (17), we find that $v_0 = \frac{1}{2}(v_u + v_w) \rightarrow v_u - v_w = 2(v_u - v_0)$.

The power

$$P = \frac{1}{2}\rho A v_0 (v_u^2 - v_w^2), \tag{18}$$

now become

$$P = \frac{1}{2}\rho A v^3 4a(1-a)^2. \tag{19}$$

Where $a = 1 - \frac{v_0}{v_u}$ is called the axial induction factor (Munteanu et al., 2014).

The power coefficient C_p given by $C_p = P/P_t$ where $P_t = \frac{1}{2}\rho A v^3$ is the ideal theoretical power now becomes

$$C_p = 4a(1-a)^2. \tag{20}$$

A C_p value of 0.59 is the maximum possible value and is called the Betz limit wish corresponds to the maximum energy extracted from the wind. C_p value of 0.59 corresponds to an induction factor $a = 1/3$ (Munteanu et al., 2014).

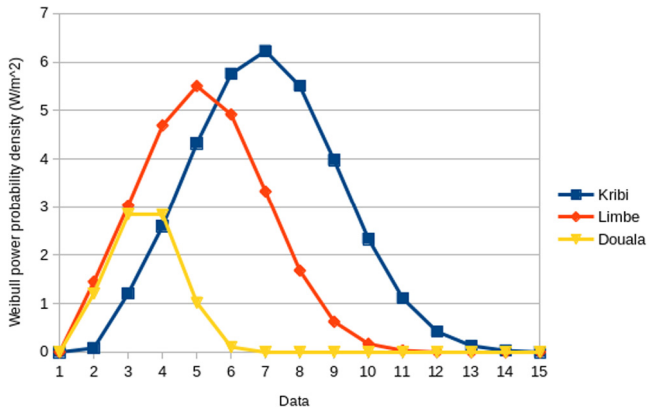

Fig. 2. A comparative plot of Weibull power density over Douala, Limbe, and Kribi.

2.3. PARK model

The PARK model assumes a linear expansion of the wake behind a wind turbine as shown in Fig. 5 with the wake velocity at a distance x down stream given by (Wang et al., 2016b; Kusiak and Song, 2010; Song et al., 2013; Samorani, 2014; Jensen, 1983; Katic et al., 1986):

$$v_x = v_0\left[1 - 2a\left(\frac{r_r}{r_r + \alpha x}\right)^2\sqrt{\frac{A_w}{A_r}}\right], \tag{21}$$

where a is the axial induction factor, r_r is the downstream rotor radius, A_w is the overlap area due to the wake effect and A_r is the turbine area of cross section. α is the wake spreading coefficient which depends on the surface roughness length z_0 and the wind turbine hub height h given by the expression (Wang et al., 2016b; Samorani, 2014):

$$\alpha = \frac{0.5}{\ln\left(\frac{h}{z_0}\right)}. \tag{22}$$

Downstream rotor radius is given by (Wang et al., 2016b):

$$r_r = R\sqrt{\frac{1-a}{1-2a}}, \tag{23}$$

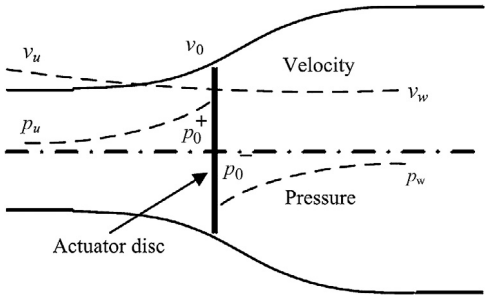

Fig. 4. Actuator disc concept.

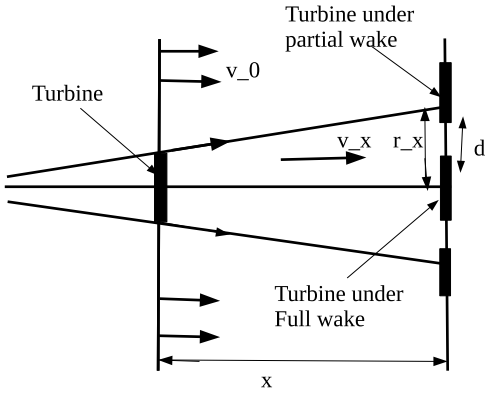

Fig. 5. An illustration of PARK model showing full and partial wake cases.

where R is the rotor radius. The wake radius down stream is given by

$$r_x = r_r + \alpha x. \tag{24}$$

For full wake layout, the area of overlap A_w is same as rotor area A_r. Hence the wake velocity for full wake becomes

$$v_x = v_0\left[1 - 2a\left(\frac{r_r}{r_r + \alpha x}\right)^2\right], \tag{25}$$

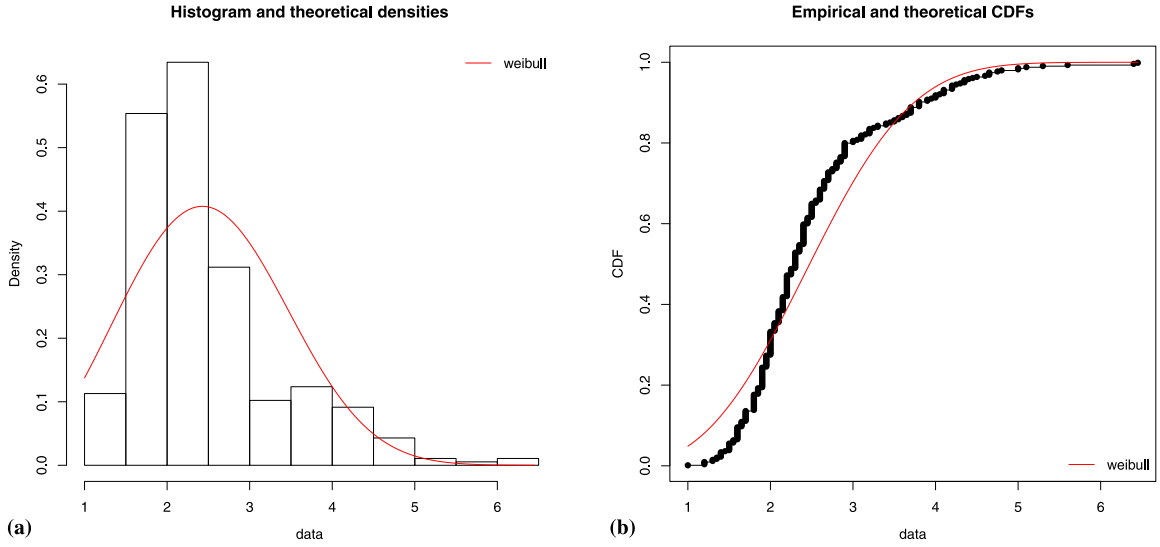

Fig. 3. Weibull probability wind speed distribution of NASA satellite data of Kribi. (a) is the probability density function and (b) is the cumulative distribution function.

with the term

$$v_{def} = 2a\left(\frac{r_r}{r_r + \alpha x}\right)^2 \tag{26}$$

call the velocity deficit for full wake (Wang et al., 2016b). from Eq. (26), we see that the $v_{def} \to 0$ as $x \to \infty$. Hence velocity deficit disappears at larger distance of separations between turbines and $v_x \approx v_0$. For partial wake, the area of overlap A_w is given by (Wang et al., 2016b):

$$A_w = r_x^2\left[\cos^{-1}\left(\frac{r_x^2 + d^2 + \triangle h^2 - R^2}{2r_x\sqrt{d^2 + \triangle h^2}}\right) - \frac{\sin\left(2\cos -1\left(\frac{r_x^2 + d^2 + \triangle h^2 - R^2}{2r_x\sqrt{d^2 + \triangle h^2}}\right)\right)}{2}\right] + R^2\left[\cos^{-1}\left(\frac{R^2 + d^2 + \triangle h^2 - r_x^2}{2R\sqrt{d^2 + \triangle h^2}}\right) - \frac{\sin\left(2\cos -1\left(\frac{R^2 + d^2 + \triangle h^2 - r_x^2}{2R\sqrt{d^2 + \triangle h^2}}\right)\right)}{2}\right] \tag{27}$$

with velocity deficit v_{def} given by,

$$v_x = v_0\left[1 - 2a\left(\frac{r_r}{r_r + \alpha x}\right)^2\sqrt{\frac{A_w}{A_r}}\right]. \tag{28}$$

This is for the case of a wind turbine under a single wake. For the case of a wind turbine under multiple wakes, the velocity deficit is given by (Wang et al., 2016b):

$$v_{def_i} = \sqrt{\sum_{r=1}^{N}\left(2a\left(\frac{r_r}{r_r + \alpha x}\right)^2\sqrt{\frac{A_w}{A_r}}\right)^2}. \tag{29}$$

The wake velocity due to these wind turbines is given by

$$v_i = v_0(1 - v_{def_i}) \tag{30}$$

A single wind turbine power according to the onshore wind turbine power curve is given by,

$$P = \frac{1}{2}\rho A v^3 C_p, \tag{31}$$

where v is the velocity that depends on the wind farm layout model. For the case of zero wake affect, v is the free stream velocity and for the case of a partial or full wake, v is the wake velocity in full or partial wake. The total power from the farm is given by,

$$P_{tot} = \sum_{i=1}^{N} P_i \tag{32}$$

where N is the number of wind turbines. As an example, let us consider a case where the area of overlap for partial wake $A_w = 0.7A_r$. The wake velocity becomes $v_x = 0.314v_0$. Full wake is for the case where $A_w = A_r$ with wake velocity $v_x = 0.297v_0$. Taking $\rho = 1.225$ kg/m^3, $r_r = 10$ m, $a = 0.33$, $z_0 = 0.01$, $h = 40$ m, $x = 100$ m and $C_p = 0.5$. The power of one wind turbine under the influence of partial wake become $P_i = 2.99$ kW and $P_i = 2.52$ kW for full wake. The estimated power from the wind farm is given by,

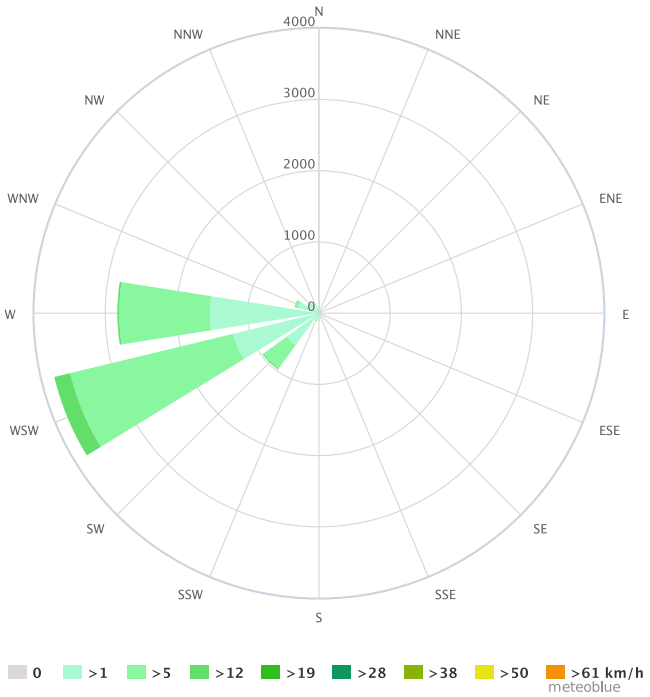

Fig. 6. Wind rose of Kribi showing dominant wind directions.

$$P_{tot} = \sum_{i=1}^{N} P_{i0} + \sum_{i=1}^{N} P_{ix}, \tag{33}$$

where P_{i0} is the power from the first row of wind turbines with no wake effect and P_{ix} is the power from other wind turbines assuming all experience partial wake. So for no wake effect, the total power from the farm is calculated to be $P_{tot} = 500$ kW. For partial wake, the total power from the farm is calculated to be $P_{tot} = 330.7$ kW and for full wake, the total power is $P_{tot} = 288.4$ kW.

2.4. Wind turbine positioning

A wind rose is a graphic tool used by scientist to give a succinct view of how wind speed and direction are typically distributed at a particular location. They are very useful in that, they give the direction of wind flow at a particular period of time which greatly helps for wind turbine positioning for maximum energy capture. The wind rose for Kribi in Fig. 6 shows that wind appears to be blowing from both the Southwest and West direction with West-South-West being the dominant wind direction. Hence East-North-East square wind farm positioning with wind turbine upstream facing West-South-West is the best for maximum energy capture.

2.5. Sizing and layout models

For sizing, we assume the availability of a 1 km × 1 km flat piece of land for the installation of 100 5 kW wind turbines with rotor radius of 10 m and same hub height of 40 m. The turbines are placed 100 m apart which gives us the ideal positioning of at least 5 blade diameter distance apart.

Now, the way wind turbines are positioned for minimal wake effect and maximizing the total wind energy production from the farm is the main area of focus for this work. Many researchers have used different wake models and advance computer simulation software like Computational Fluid Dynamics (CFD) to study different wake models and layout models that will drastically reduce the

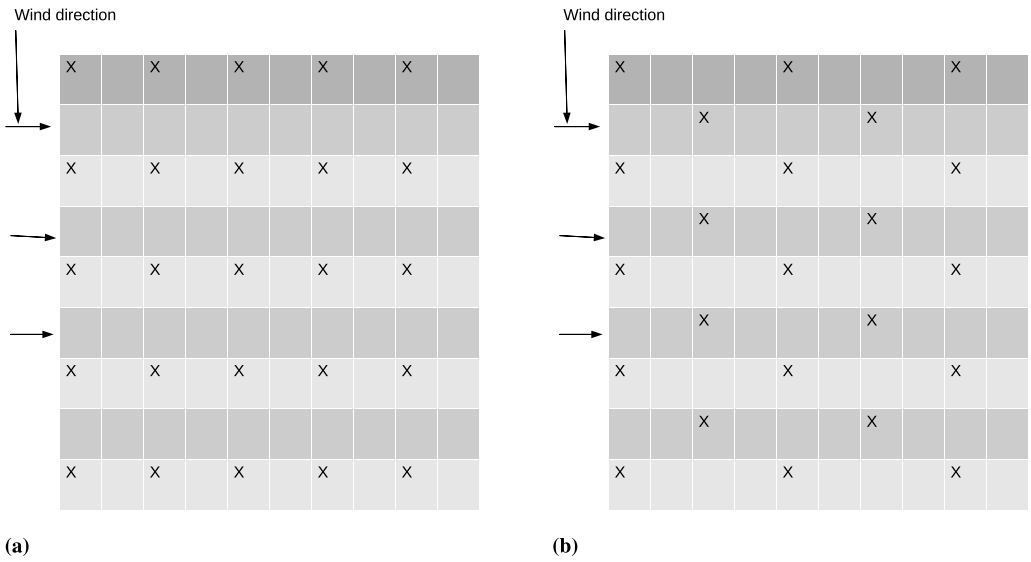

Fig. 7. An illustrated case of wind turbine layout patten (a) is the column model for full wake and (b) is the checkers model for partial wake. 'X' represents the wind turbine.

wake effect while economizing total space to be used (Samorani, 2014; Jensen, 1983; Katic et al., 1986; Feng and Shen, 2015; Wang et al., 2016a, 2015; Frandsen, 1992; Shahriar et al., 2015). Here, we have used the most popular and widely used model for wind farm optimization layout which is the PARK model.

Users of the PARK model through computer simulation using CFD have found that this model experience the maximum possible wake effect called full wake for wind turbines placed in column patten. Other wind farm developers have found that irregular arrangement of wind turbines in a farm have more wake minimization than wind turbines arranged in columns. So our model of the wind farm stems from the game of checkers. A checkers pattern is shown in Fig. 7b. Our idea is that while using same dimension of land, the second row of wind turbines are placed at mid distance of the two neighbouring turbines in the first row while those in the 3rd row are also placed at mid point between tow neighbouring turbines in the second row and are on same column as those in the first row. Also working on the assumption that the wake effect is drastically reduced at wider distances between two turbines on same column, only partial wake is experienced in this checkers layout model.

3. Results and discussion

We have previously compared wind energy potentials of three cities in three different coastal regions of Cameroon and found that Kribi in the South region is the best site (Arreyndip et al., 2016). We also proposed the use of Savonius wind turbines for stand alone low energy needs. But this site can also support small wind turbines up to 100 kW. Table 4 shows a suggestion of the wind turbine to be used, its parameter specifications and total cost including shipping and installation. In Figs. 8 and 9, using the PARK model, we study the effects of distance(x) from the wind turbine upstream of the wake on wake velocity at different surface roughness as shown in Fig. 8a. Here, we see that the surface roughness has a very small effect on the wake velocity but greatly affects the velocity deficit for full wake as shown in Fig. 8b.

Fig. 9a studies the effect of surface roughness on velocity deficit for partial wake which is similar to that of full wake but with a slight decrease. In Fig. 9b, power deficit for partial and full wake are compared at a surface roughness of $z = 0.001$. We see that the power deficit is slightly less in partial wake layout as compared to full wake layout. The various layout pattens are shown in Fig. 7a for column layout that accounts for full wake and Fig. 7b for Checkers layout that accounts for partial wake which is based on the assumption that, the further downstream a wind turbine is from a wake, the lesser it experiences the wake effect and hence the wake velocity approaches the free stream velocity. In the last part of Section 2.3, we have calculated and compared the total power output of the farm in different three layout patterns. Here, we see that the ideal layout of wind turbines is for all wind turbines to be placed in a row which gives an estimated power of 500 kW. But this layout model will take an incredible amount of space. The next best layout model is the Checkers model with an estimated power of 330.7 kW and finally the column model with an estimated power of 288.4 kW. The estimated power can then be met by using an appropriate step-up transformer.

Table 4
Small wind farm estimated parameters and installation cost.

Parameters	Values
Wind Farm estimated power	500 kW
1 Wind turbine power	5 kW
Number of wind turbines	100
Rotor diameter	20 m
hub height	40 m
Cut-in-speed	2.0 m/s
Rated speed	8 m/s
Cut-out-speed	12 m/s
Total cost (shipping plus installation) for 1 turbine	$15,000
100 turbines cost	$1,500,000
Average cost of 1 m^2 of land	$20
Total cost of land	$20,000,000
Total project cost	$21,500,000

Finally, Fig. 10 is a google map showing the position where the wind farm is to be constructed at Grand Batanga locality in Kribi. We estimated the availability of a 1 km $\times$ 1 km square piece of land that will be taken away from the indigents and compensated by funds allocated in Table 4. Fig. 11 is a satellite map showing positioning of the farm and Checkers model layout patten over the site following wind direction from wind rose of Kribi.

4. Conclusion

Due to mass migration of working population from landlocked regions to the coastal regions in search of jobs and a better livelihood, the population of these coastal regions is increasing yearly

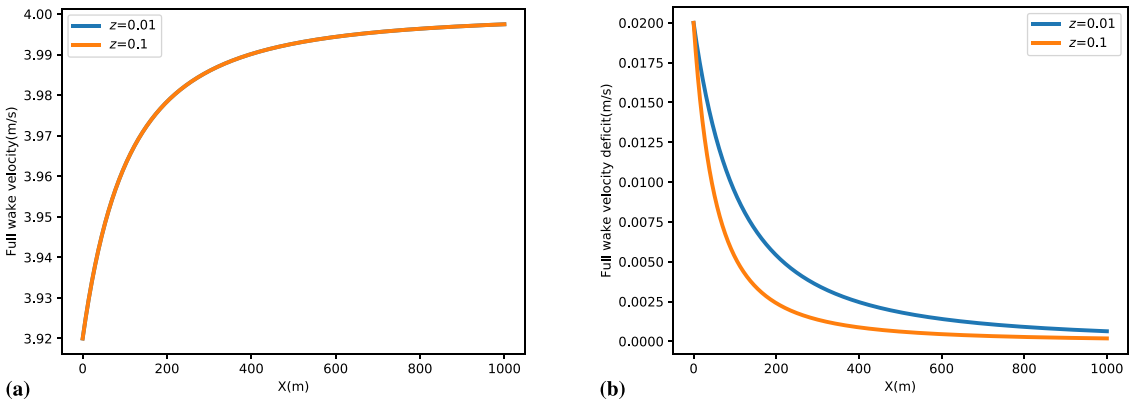

Fig. 8. (a) is a plot of full wake velocity against distance from wind turbine at different values of the surface roughness. (b) is a plot of the velocity deficit at a distance from the turbine at different values of the surface roughness.

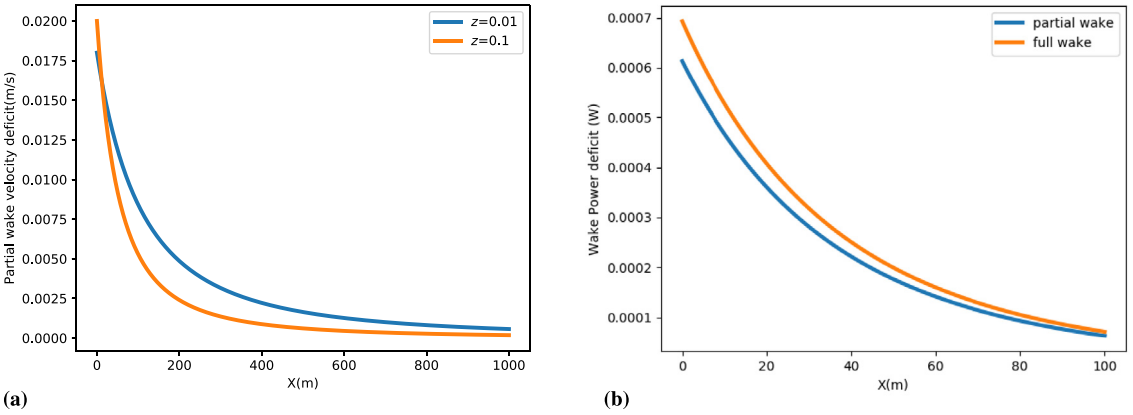

Fig. 9. (a) is a plot of partial wake velocity deficit against distance from wind turbine at different values of the surface roughness. (b) is a plot of wake power deficit comparing full wake with partial wake at a distance from the turbine.

Fig. 10. Google image of Kribi showing chosen site for wind farm installation.

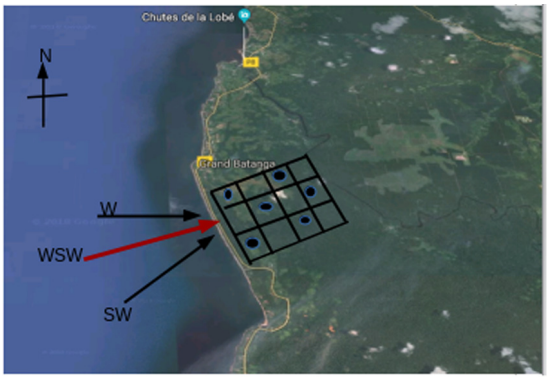

Fig. 11. Wind farm positioning south of Grand Batanga using the checkers model.

in an alarming rate. Also to become an emerging state by the year 2035, the government of Cameroon has heavily invested in industrialization. There is therefore the demand for more and more energy. To solve these ever increasing energy crises in the densely populated coastal cities, a thorough wind energy potential has been carried out to identify a potential site for the installation of a small onshore wind farm. Kribi has been found suitable and the wind speed characteristics over Kribi, shows that it can only support a wind farm made up of small wind turbines. We have estimated the power output from this wind farm of dimension 1 km $\times$ 1 km to be 500 kW. We have proposed the installation of 100 5 kW (with rotor diameter of 20 m) wind turbines to meet this estimated power.

To harvest maximum power from the farm, we have applied the PARK model for wind turbine layout optimization. We have studied two different layout pattens which are the column layout pattern where the wind turbines are laid out in columns in the farm and the Checkers layout pattern (being inspired from the game of Checkers) where wind turbines of the next row are displaced half the distance of separation between turbines of the previous row. Through calculations, we have seen that the Checkers layout is better than the column pattern in minimizing the wake effect and thereby maximizing the total output power from the farm.

Acknowledgements

This work was supported by the government of Canada's International Development Research Centre (IDRC), and within the framework of the AIMS Research for Africa Project (CMMCM2014025S).

The authors will like to thank Prof. Alain Moise Dikande, head of the LaRaManS research group of the Department of Physics, University of Buea for fruitful discussions that let to solid ideas used to produce this manuscript.

References

Akpinar, E.K., Akpinar, S., 2005. An assessment on seasonal analysis of wind energy characteristics and wind turbine characteristics. Energy Convers Manage 46, 1848e67.

Anon, 2014. Vestas Wind Systems A/S, derived from International Energy Agency (IEA), the World Bank and Vestas data https://www.africa-eu-renewables.org/market-information/cameroon/renewable-energy-potential/.

Archer, C.L., Mirzaeisefat, S., Lee, S., 2013. Quantifying the sensitivity of wind farm performance to array layout options using large-eddy simulation. Geophys. Res. Lett. 40 (18), 4963–4970.

Arreyndip, Nkongho Ayuketang, Joseph, Ebobenow, 2016. Generalized extreme value distribution models for the assessment of seasonal wind energy potential of Debuncha, Cameroon. J. Renew. Energy 9357812, 9, http://dx.doi.org/10.1155/2016/9357812.

Arreyndip, Nkongho Ayuketang, Joseph, Ebobenow, David, Afungchui, 2016. Wind energy potential assessment of Cameroon's coastal regions for the installation of an onshore wind farm. Heliyon 2, e00187. http://dx.doi.org/10.1016/j.heliyon.2016.e00187.

Carta, J.A., Ramıez, P., Velázquez, S., 2009. A review of wind speed probability distributions used in wind energy analysis: case studies in the Canary Islands. Renew. Sustain. Energy Rev. 13, 933e55.

Castellani, F., et al., 2013. A practical approach in the cfd simulation of off-shore wind farms through the actuator disc technique. Energy Proc. 35, 274–284.

Fagbenle, R.O., et al., 2011. Assessment of wind energy potential of two sites in North-East, Nigeria. Renew. Energy 36, 1277–1283.

Feng, J., Shen, W.Z., 2015. Solving the wind farm layout optimization problem using random search algorithm. Renew. Energy 78, 182–192.

Frandsen, S., 1992. On the wind speed reduction in the centre of large clusters of wind turbines. J. Wind Eng. Ind. Aerodyn. 39 (1), 251–265.

Jensen, N.O., 1983. A note on wind generator interaction.

Katic, I., Højstrup, J., Jensen, N., 1986. A simple model for cluster efficiency.

Kollu, et al., 2012. Mixture probability distribution functions to model wind speed distributions. Int. J. Energy Environ. Eng. 3, 27, http://www.journal-ijeee.com/content/3/1/27.

Kusiak, A., Song, Z., 2010. Design of wind farm layout for maximum wind energy capture. Renew. Energy 35 (3), 685–694.

Montgomery, D.C., Runger, G.C., 2003. Applied Statistics and Probability for Engineers, third ed. Wiley, New Jersey.

Munteanu, I., Bratcu, A.I., Cutululis, N.-A., Ceanga, E., 2014. Optimal Control of Wind Energy Systems. Towards a Global Approach, Springer, pp. 15–16 (Chapter 2). http://www.springer.com/gp/book/9781848000797.

Oyedepo, et al., 2012. Analysis of wind speed data and wind energy potential in three selected locations in south-east Nigeria. Int. J. Energy Environ. Eng. 3, 27, http://www.journal-ijeee.com/content/3/1/7.

Ozerdem, B., Turkeli, M., 2003. An investigation of wind characteristics on the campus of Izmir Institute of Technology, Turkey. Renew. Energy 28, 1013e27.

Samorani, Michele, 2014. Michele Samorani The Wind Farm Layout Optimization Problem. Springer, p. 16, https://link.springer.com/chapter/10.1007/978-3-642-41080-2_2.

Shahriar, M.R., et al., 2015. Fault detection of wind turbine drivetrain utilizing power- speed characteristics. In: 9th WCEAM Research Papers. Springer, pp. 143–155.

Song, M.X., et al., 2013. Bionic optimization for micro-siting of wind farm on complex terrain. Renew Energy 50, 551–557.

Wang, Longyan, Tan, Abdy C.C., Cholette, Michael, Gu, Yuantong, 2016b. Comparison of the effectiveness of analytical wake models for wind farm with constant and variable hub heights. Energy Convers. Manage. 124, 189–202.

Wang, L., Tan, A., Gu, Y., 2016a. A novel control strategy approach to optimally design a wind farm layout. Renew. Energy 95, 10–21.

Wang, L., et al., 2015. A new constraint handling method for wind farm layout optimization with lands owned by different owners. Renew. Energy 83, 151–161.